The Company of **Biologists**

RESEARCH ARTICLE

Disrupting the three-dimensional regulatory topology of the *Pitx1* locus results in overtly normal development

Richard Sarro[1], Acadia A. Kocher[1], Deena Emera[1], Severin Uebbing[1], Emily V. Dutrow[1], Scott D. Weatherbee[1], Timothy Nottoli[2,3] and James P. Noonan[1,*]

ABSTRACT

Developmental gene expression patterns are orchestrated by thousands of distant-acting transcriptional enhancers. However, identifying enhancers essential for the expression of their target genes has proven challenging. Maps of long-range regulatory interactions may provide the means to identify enhancers crucial for developmental gene expression. To investigate this hypothesis, we used circular chromosome conformation capture coupled with interaction maps in the mouse limb to characterize the regulatory topology of *Pitx1*, which is essential for hindlimb development. We identified a robust hindlimb-specific interaction between *Pitx1* and a putative hindlimb-specific enhancer. To interrogate the role of this interaction in *Pitx1* regulation, we used genome editing to delete this enhancer in mouse. Although deletion of the enhancer completely disrupts the interaction, *Pitx1* expression in the hindlimb is only mildly affected, without any detectable compensatory interactions between the *Pitx1* promoter and potentially redundant enhancers. *Pitx1* enhancer null mice did not exhibit any of the characteristic morphological defects of the *Pitx1*⁻/⁻ mutant. Our results suggest that robust, tissue-specific physical interactions at essential developmental genes have limited predictive value for identifying enhancer mutations with strong loss-of-function phenotypes.

KEY WORDS: Enhancer-promoter interactions, Genomics, Limb development, Enhancer loss-of-function mutations

INTRODUCTION

Embryonic development depends on the spatial, temporal, and quantitative control of gene expression. The complex regulatory programs that orchestrate morphogenesis are specified by thousands of tissue-specific, distant-acting enhancers, which are brought into contact with their gene targets via long-range chromatin looping interactions (Tolhuis et al., 2002; Pennacchio et al., 2006; Visel et al., 2009; Fullwood et al., 2009; Noonan and McCallion, 2010; Montavon et al., 2011; Sanyal et al., 2012; de Laat and Duboule, 2013; DeMare et al., 2013; Shlyueva et al., 2014; Ghavi-Helm et al., 2014; Rao et al., 2014). These contacts occur within stable, megabase-scale topologically associated domains (TADs), many of which are conserved across tissues and species (Dixon et al., 2012; Nora et al., 2012; Phillips-Cremins et al., 2013; Lupiáñez et al., 2015).

Despite their clear overall importance for development, quantifying the contribution of individual enhancers to the expression of their target genes has been difficult. Genetic knockout studies of single enhancers in the mouse have yielded a range of molecular and phenotypic effects. In a classic example, deletion of the ZRS, a long-range enhancer that controls expression of *Shh* specifically in the developing limb bud, results in loss of *Shh* expression and truncation of the mouse limb (Lettice et al., 2003; Sagai et al., 2005). However, knockouts of other enhancers near developmental genes show less severe phenotypes (Attanasio et al., 2013; Dickel et al., 2016, 2018) or no obvious phenotype at all (Ahituv et al., 2007).

One potential mechanism to account for this result is that many developmental genes are regulated by multiple, redundant enhancers with overlapping functions that may compensate for the loss of a single enhancer (Hong et al., 2008; Degenhardt et al., 2010; Frankel et al., 2010; Perry et al., 2010; Montavon et al., 2011; Cannavò et al., 2016; Osterwalder et al., 2018). This redundancy potentially serves to buffer the effects of genetic disruptions of individual enhancers. Clearly, however, the loss of some enhancers cannot be buffered; the ZRS appears to be the primary source of regulatory information for specifying *Shh* expression in the limb bud (Lettice et al., 2003; Sagai et al., 2005). Identifying such crucial enhancers that are likely to exhibit overt loss-of-function phenotypes when disrupted has been challenging. Evolutionary conservation, tissue-specific chromatin signatures, and activity in transgenic reporter assays have all been used to map developmental enhancers in the genome (Noonan and McCallion, 2010). However, these metrics have not provided the means to distinguish enhancer mutations with large effects from mutations that can be buffered by compensatory mechanisms. This presents a major barrier for efforts to understand the contribution of regulatory variation to human disease.

We hypothesized that topological interactions would be a useful filter, in that individual enhancers crucial to tissue-specific expression of pleiotropic developmental genes would show robust, tissue-specific interactions with those targets. In this way, topology may be used to identify not just an enhancer's targets, but also to predict the potential effects of an enhancer deletion. Supporting this hypothesis, it has been shown that the ZRS interacts with *Shh* in the limb bud (Amano et al., 2009; Williamson et al., 2016) and that *HoxD* gene expression in the developing limb is specified by an array of interacting enhancers (Montavon et al., 2011). To identify potentially essential developmental enhancers, we leveraged the results of a recent study that utilized chromatin interaction analysis by paired-end tag sequencing (ChIA-PET) targeting the SMC1A cohesin subunit to identify over 2500 cohesin-bound chromatin loops in E11.5 mouse limb (DeMare et al., 2013). From this study, we identified a robust, hindlimb-specific interaction between the pleiotropic developmental gene *Pitx1* and a sequence located 132 kb away, which we termed the *Pitx1* distal enhancer (PDE).

[1]Department of Genetics, Yale School of Medicine, New Haven, CT 06520, USA. [2]Department of Comparative Medicine, Yale School of Medicine, New Haven, CT 06520, USA. [3]Yale Genome Editing Center, Yale School of Medicine, New Haven, CT 06520, USA.

*Author for correspondence (james.noonan@yale.edu)

R.S., 0000-0003-2054-5369; D.E., 0000-0003-1034-3464; J.P.N., 0000-0001-9632-5835

DEVELOPMENT

Pitx1 encodes a homeodomain transcription factor prominently expressed in the hindlimb and mandibular arch (Szeto et al., 1999; Lanctôt et al., 1999). *Pitx1*$^{+/−}$ mice are overtly normal, exhibiting only minor morphological defects at low levels of penetrance (Alvarado et al., 2011). *Pitx1*$^{−/−}$ mice show early postnatal lethality, as well as loss of the ilium, a reduction in length of the femur, a loss of the patella, and a reduced, malformed mandible (Szeto et al., 1999; Lanctôt et al., 1999). *Pitx1* is hypothesized to establish hindlimb identity, and overexpression of *Pitx1* in the forelimb produces a hindlimb-like morphology (Logan and Tabin, 1999). Prior studies have identified *Pitx1* enhancer mutations that result in substantial morphological phenotypes in non-mammalian systems (Chan et al., 2010; Domyan et al., 2016). We predicted that loss of the PDE may also have substantial molecular and morphological effects. The PDE displays strong, hindlimb-specific H3K27ac marking, a signature of active enhancers; in the forelimb the sequence is marked by H3K27me3, which is associated with PRC2-mediated repression (Cotney et al., 2012). The PDE is also highly conserved across amniote species, suggesting that it serves an ancient role in *Pitx1* regulation.

We used CRISPR/Cas9 to delete the PDE in the mouse, thus abolishing any regulatory input or topological insulation conferred by the interaction. We anticipated two potential outcomes from the loss of the PDE: the recapitulation of morphological defects observed in *Pitx1* null mice, or the formation of aberrant and/or compensatory interactions between *Pitx1* and other potential regulatory elements in the absence of the primary interaction. Instead, we found PDE loss to have only mild effects on *Pitx1* expression in the hindlimb and no overt effects on hindlimb or mandibular morphology. No changes in enhancer activity or new long-range interactions were identified, at least at a level detectable by our methods, that might have compensated for the loss of the PDE.

RESULTS
Mapping *Pitx1* regulatory interactions
We first characterized the topological landscape of the *Pitx1* promoter in the mouse embryonic forelimb and hindlimb using circularized chromosome conformation capture (4C) (Simonis et al., 2006). We were able to recapitulate the previously described *Pitx1*-PDE interaction in the wild-type mouse E11.5 hindlimb. This interaction is the most prominent topological interaction we identified involving the *Pitx1* promoter in the genome (FourCSeq replicate 1 P=0.00754, replicate 2 P=0.00374; see Materials and Methods; Fig. 1, Table S1). *Pitx1* also interacts with the PDE at a low level in the E11.5 forelimb (FourCSeq replicate 1 P=0.03067, replicate 2 P=0.05542). These interaction frequencies correlate with the expression levels of *Pitx1* and the epigenetic profile of the enhancer in the hindlimb and forelimb. In the hindlimb, *Pitx1* is expressed and the PDE exhibits high levels of
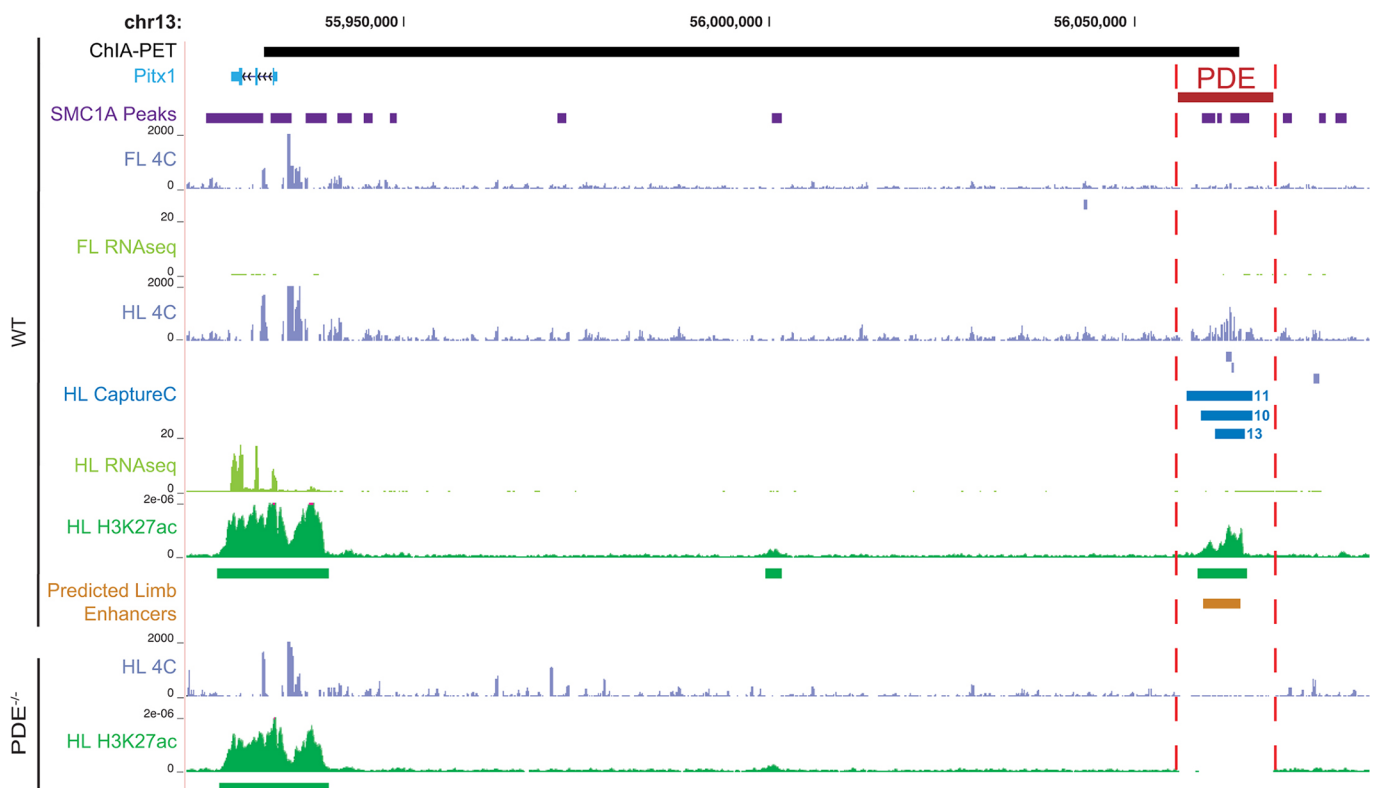

Fig. 1. *Pitx1*-PDE interaction in mouse E11.5 limb buds. (Top) 4C interaction profiles of the *Pitx1* promoter in wild-type forelimb (FL) and hindlimb (HL) are shown in light blue. Reproducible, nominally significant interacting regions as called by FourCSeq are shown below each track. Transcription profiles (RNA-seq) in forelimb and hindlimb are shown in light green, and H3K27ac signal and enriched regions in hindlimb are shown in dark green. The ChIA-PET interaction between *Pitx1* and the PDE previously identified in E11.5 limb buds is shown in black at the top of the figure, and SMC1A binding sites are shown in purple (DeMare et al., 2013). Interactions detected by Andrey et al. (2017) between the *Pitx1* promoter and the PDE in embryonic mouse hindlimb are shown in dark blue; the numbers refer to each embryonic time point at which an interaction was detected. Enhancers predicted to be active in the embryonic limb by Monti et al. (2017) are shown in orange. The location of the PDE (chr13:56,055,928-56,068,947 in mm9) is shown in red. (Bottom) *Pitx1* promoter interaction profile and H3K27ac signal in PDE$^{−/−}$ E11.5 hindlimb.

H3K27ac (Fig. 1). Conversely, *Pitx1* is not expressed in the forelimb, and both the *Pitx1* promoter and the PDE sequence are marked by H3K27me3, indicating they are repressed in this tissue (Cotney et al., 2012).

To further characterize the regulatory landscape of the *Pitx1* locus, we turned to a recent study that incorporated multiple functional and comparative genomic datasets to predict enhancers likely to be active in the limb (Monti et al. (2017). This study identified 31 predicted enhancers within the TAD that encompasses *Pitx1*, including the PDE (see Fig. 4 and Fig. S1). To determine whether these additional enhancers interact with the *Pitx1* promoter, we analyzed Capture-C interaction maps obtained from mouse embryonic limb (Andrey et al., 2017). This study identified interactions between the *Pitx1* promoter and the PDE in the hindlimb at multiple developmental time points (Fig. 1). This study also identified *Pitx1* promoter interactions with four additional loci (Fig. S1), which we did not detect using 4C. One of these interactions involved the promoter of a nearby gene, *H2afy*. Three others involved putative limb enhancers, all of which showed H3K27ac marking in E11.5 forelimb and hindlimb, including a sequence shown to drive reporter gene expression in embryonic mouse forelimb and hindlimb at this time point (Fig. S2) (Pennacchio et al., 2006). However, the PDE shows significantly greater marking in hindlimb compared with forelimb (Fig. S1) (Cotney et al., 2012), and its strong, hindlimb-specific interaction with *Pitx1* has been detected by multiple independent methods, suggesting that it might substantially contribute to the hindlimb-specific expression pattern of *Pitx1*.

Generation and validation of PDE$^{-/-}$ mice
In order to disrupt the *Pitx1*-PDE interaction, we used CRISPR/Cas9 genome editing to generate a Cre-loxP conditional deletion allele in C57BL6/J mice (Figs S2 and S3). The locations of the loxP insertions were designed to ensure that all local SMC1A binding sites identified would be removed (DeMare et al., 2013). We first validated the deletion of the PDE sequence via PCR and Sanger sequencing (Fig. S1). We then validated the ablation of the topological interaction using 4C (Fig. 1). The loss of the PDE sequence is also evident as a lack of sequencing reads in the deleted interval in limb H3K27ac ChIP-seq and 4C datasets (Fig. 1). We did not detect any evidence of increased interaction frequency in the genomic regions flanking the deletion, supporting that removal of the PDE completely disrupts the promoter-enhancer interaction.

Although *Pitx1*$^{-/-}$ mice exhibit neonatal lethality, we did not observe any reduction in viability in constitutive PDE$^{-/-}$ mice. PDE$^{+/-}$×PDE$^{+/-}$ crosses yielded wild-type, PDE$^{+/-}$ and PDE$^{-/-}$ offspring at the expected 1:2:1 ratio (Table S2). We therefore compared wild-type and constitutive PDE homozygous knockout mice in all subsequent analyses.

Comparison of *Pitx1* expression in wild-type and PDE$^{-/-}$ mice
We next considered the effects of the PDE deletion on *Pitx1* expression. We examined two tissues that are known to both express *Pitx1* during embryonic development and exhibit malformations in *Pitx1*$^{-/-}$ mice: the hindlimb and the mandibular arch. To analyze *Pitx1* expression, we initially compared hindlimbs and mandibular arches from litter-matched wild-type and PDE$^{-/-}$ mice using RT-qPCR (Fig. 2, Fig. S4). We carried out a timecourse analysis of *Pitx1* expression in the hindlimb from E10.5 through E13.5. *Pitx1* expression was reduced by 13-16% in PDE$^{-/-}$ hindlimb at all four time points. This reduction was a significant effect of the PDE deletion, and not solely attributable to litter effects or variation
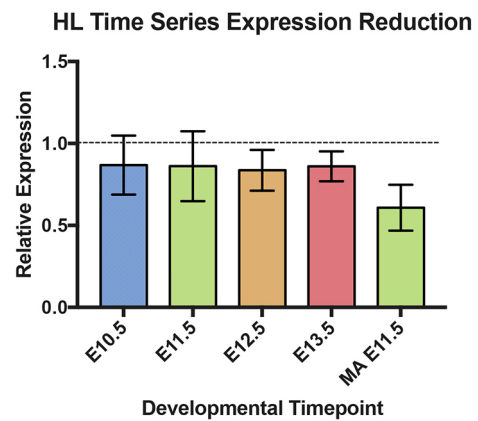

Fig. 2. Reduced *Pitx1* expression in PDE$^{-/-}$ embryonic hindlimb and mandibular arch. Relative *Pitx1* expression in PDE$^{-/-}$ hindlimb at four time points (E10.5-E13.5) and E11.5 mandibular arch (MA) measured using RT-qPCR. *Pitx1* expression in PDE$^{-/-}$ relative to wild-type tissues was calculated by the $^{\Delta\Delta}$Ct method, using *Hprt1* as an internal reference. Error bars represent $2^{-(\Delta\Delta Ct \pm stdevwtHPRT1)}$.

across developmental time points (three-way mixed effect ANCOVA $F_{1,20}$=18.624, P=3.36×10^{-4}; Fig. 2; see Materials and Methods). We also carried out pairwise comparisons at each time point, which indicated that *Pitx1* expression was significantly reduced in PDE$^{-/-}$ hindlimb at E12.5 and E13.5 (Mann–Whitney U-test P=0.012 and P=0.021, respectively; Fig. S4) (Mann and Whitney, 1947). Loss of *Pitx1* expression was more substantial in PDE$^{-/-}$ E11.5 mandibular arch than in hindlimb (39% expression reduction, Mann–Whitney U-test P=8.6×10^{-4}).

We then performed RNA-seq in wild-type and PDE$^{-/-}$ hindlimb and mandibular arch at E11.5 to identify potential global changes in gene expression due to reduced *Pitx1* levels. In PDE$^{-/-}$ mice, *Pitx1* showed a similar reduction in expression in both tissues, as we observed by RT-qPCR (14.5% in hindlimb, 32.14% in mandibular arch; Tables S3, S4). However, the change of expression in each tissue was not statistically significant after multiple testing correction [hindlimb DESeq Benjamini–Hochberg corrected (BH) P=0.9997, mandibular arch DESeq BH P=0.5946 (Anders and Huber, 2010)]. Expression of *Tbx4*, a known downstream regulatory target of *Pitx1* in the hindlimb (Logan and Tabin, 1999), was reduced by 4.68% (P=0.295, BH P=0.9997). Our DESeq analysis did not identify any genes to be significantly altered in expression between wild type and PDE$^{-/-}$ after multiple testing correction in either tissue (at a threshold of BH P<0.05).

To gain insight into potential subtle effects of *Pitx1* reduction of expression, we conducted gene ontology (GO) enrichment analyses of all genes exhibiting expression changes with a non-adjusted P-value <0.05 (271 hindlimb genes, 234 mandibular arch genes; Table S5). Genes that met this relaxed threshold in either tissue were associated with GO categories related to embryonic development and gene regulation. However, no ontologies reached a BH adjusted P-value <1.5×10^{-7} (Huang et al., 2008). This further suggests that the reduced dosage of *Pitx1* did not cause substantial changes to regulatory networks or developmental processes in either the limb or the mandibular arch.

To determine if loss of the *Pitx1*-PDE interaction resulted in changes in the spatial distribution of *Pitx1* expression in the hindlimb and mandibular arch, we visualized *Pitx1* expression using whole-mount *in situ* hybridization on litter-matched wild-type and PDE$^{-/-}$ E11.5 embryos. In agreement with previous studies (Szeto

et al., 1999; Lanctôt et al., 1999), our *in situ* analysis detected *Pitx1* expression localized to the mandibular arch and hindlimb in wild-type embryos (Fig. 3). We observed the same pattern of expression in PDE$^{-/-}$ embryos, indicating that the spatial distribution of *Pitx1* expression at E11.5 is not substantially altered by loss of the PDE (Fig. 3, Fig. S5).

Activity of the PDE in a transgenic enhancer assay

To evaluate the tissue-specific enhancer activity of the PDE independent of its interaction with the *Pitx1* promoter or its genomic context, we used a transgenic mouse reporter assay (Pennacchio et al., 2006). We tested an 8.3 kb interval within the PDE that included the region of H3K27ac enrichment in hindlimb and all PhastCons conserved elements within the H3K27ac peak (Siepel et al., 2005). At E11.5, this sequence drove strong, reproducible *lacZ* reporter expression in the mandibular arch (four of seven positive embryos; Fig. S6). However, only three embryos showed reporter gene expression in the limb mesenchyme, and in inconsistent patterns, indicating that the PDE does not drive robust gene expression in the limb when removed from its endogenous location. These findings, together with the greater reduction of *Pitx1* expression in mandibular arch versus hindlimb in PDE$^{-/-}$ embryos, support the conclusion that the PDE only contributes moderately to *Pitx1* expression in the hindlimb despite its strong interaction with the *Pitx1* promoter.
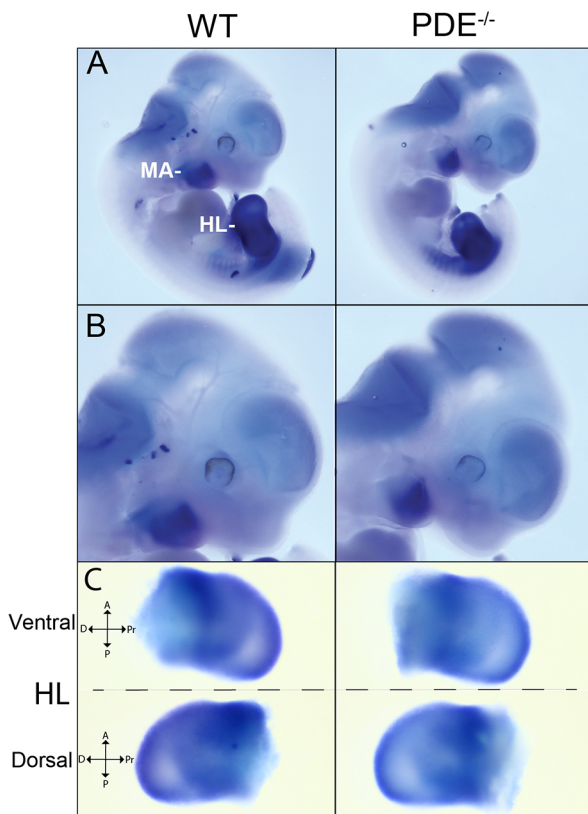

WT   PDE$^{-/-}$

Fig. 3. Spatial distribution of *Pitx1* in wild-type and PDE$^{-/-}$ E11.5 embryos. (A) *Pitx1* expression in wild-type and PDE$^{-/-}$ embryos visualized by whole-mount *in situ* hybridization. The hindlimb (HL) and mandibular arch (MA) expression domains are labeled. (B) Magnified view of *Pitx1* expression in the mandibular arch in the embryos shown in A. (C) *Pitx1* expression in wild-type and PDE$^{-/-}$ E11.5 hindlimb. Ventral and dorsal views are shown. A, anterior; P, posterior; Pr, proximal; D, distal.

Comparing epigenetic signatures of regulatory element activity between wild-type and PDE$^{-/-}$ mice

Deletion of the PDE sequence removed the major interacting partner of the *Pitx1* promoter we could detect in the hindlimb. We hypothesized that this loss would result in an unoccupied chromatin anchor point at the *Pitx1* promoter, leaving it potentially accessible to other regulatory interactions that might compensate for loss of the primary enhancer. Such compensatory events might be detected as changes in the observed interaction frequency and epigenetic profile at other loci within the TAD containing *Pitx1* (Dixon et al., 2012). We detected three 4C interactions within the *Pitx1* TAD that reached reproducible, nominal significance in PDE$^{-/-}$ hindlimbs but not in wild type (Fig. 4, Fig. S1, Table S1). However, there is little evidence that these provide novel or compensatory regulatory information to *Pitx1*. Two of these regions did not involve potential enhancers based on H3K27ac enrichment, while one involved an interaction detected by Capture-C in wild-type hindlimb (Fig. S1) (Andrey et al., 2017). Our results therefore do not support widespread or robust changes in regulatory interactions arising due to loss of the PDE (Fig. 4). As a caveat, we note that the limited sensitivity of 4C does not allow us to rule out the formation of transient chromatin interactions or interactions restricted to a subset of cells in the limb bud.

To identify potential compensatory increases in enhancer activity (independent of topology and the limitations of 4C), we used ChIP-seq to profile H3K27ac in E11.5 hindlimbs derived from wild-type and PDE$^{-/-}$ mice. Compensatory enhancer activation events may appear as new H3K27ac peaks, or as increases in H3K27ac at active enhancers. We also profiled H3K27me3 in the E11.5 PDE$^{-/-}$ and wild-type hindlimb to identify any potential changes to repressed sequences in the PDE$^{-/-}$ background. H3K27ac signatures were very similar in the wild type and PDE$^{-/-}$, both within the *Pitx1* TAD and across the genome (Fig. 4). Genome-wide, we identified 11 H3K27ac and 33 H3K27me3 regions showing statistically significant differential marking between the wild-type and PDE$^{-/-}$ samples (DESeq BH $P<0.01$; Tables S6, S7). The *Pitx1* gene body itself exhibited a significant overall loss of acetylation of ~10% in PDE$^{-/-}$ mice (DESeq BH $P=4.33\times10^{-5}$), consistent with the loss of expression that we observed. Two other significant changes in H3K27ac signal were found on chromosome 13, although neither was located within the *Pitx1* TAD. These comprised a 15% gain and a 10% loss 4.5 Mb and 25 Mb away, respectively, from *Pitx1*. Neither of these sites showed evidence of significant interactions with the *Pitx1* promoter in our 4C data in either wild-type or PDE$^{-/-}$ hindlimb. The other interacting enhancers identified by Capture-C did not show significant changes in H3K27ac levels. Thus, we found no clear evidence of regulatory compensation at *Pitx1* in E11.5 PDE$^{-/-}$ hindlimb.

Morphological analysis of PDE$^{-/-}$ mice

We also evaluated the impact of the *Pitx1* PDE deletion on skeletal morphology. Previous studies have described the complete loss of the ilium and patella in *Pitx1*$^{-/-}$ mice (Szeto et al., 1999; Lanctôt et al., 1999). These mice also exhibit a shortened hindlimb stylopod and a malformed mandible. We examined skeletal morphology in 20 PDE$^{-/-}$ mice at E18.5 using Alizarin Red/Alcian Blue staining, and none showed any of the gross anatomical defects observed in *Pitx1*$^{-/-}$ mice (Fig. 5, Figs S7 and S8). Both the overall morphology and length of the hindlimb stylopod and mandible appeared unchanged in PDE$^{-/-}$ mice.

To detect potentially subtle reductions of the hindlimb we measured the length of the stylopod and zeugopod in litter-matched
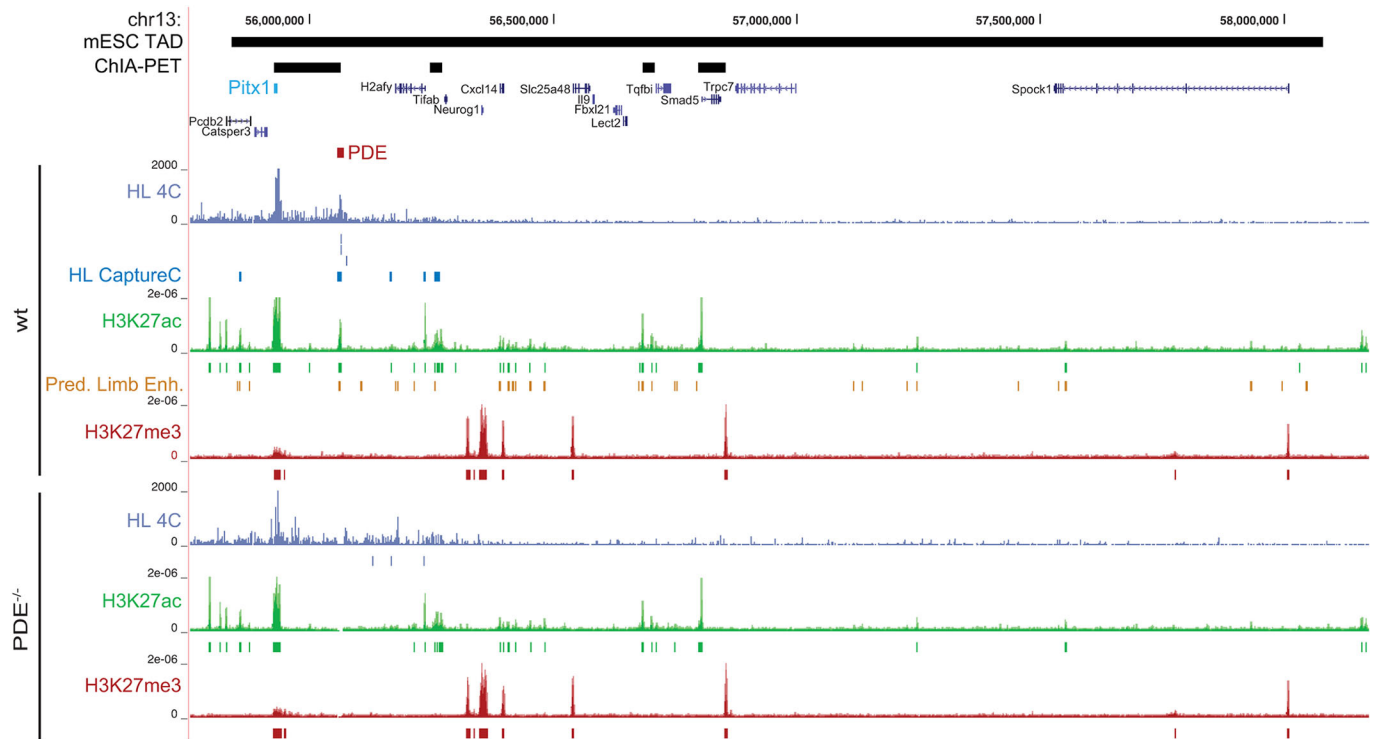
Fig. 4. Epigenetic profiles are maintained within the *Pitx1* TAD in wild-type and PDE⁻/⁻ hindlimbs. Hindlimb 4C signal tracks in wild-type and PDE⁻/⁻ mice are shown in light blue; FourCSeq peak calls are shown below each track. H3K27ac (green) and H3K27me3 (red) profiles in E11.5 hindlimb from wild-type and PDE⁻/⁻ mice are also shown. Enriched regions identified for each mark in each tissue are shown beneath each signal track. Distal *Pitx1* promoter interactions identified by Capture-C (Andrey et al., 2017) are shown in dark blue below the hindlimb 4C signal track. The TAD that encompasses *Pitx1* is shown in black at the top, as are local ChIA-PET interactions identified by DeMare et al. (2013). Enhancers predicted to be active in embryonic mouse limb are shown in orange Monti et al. (2017).

E18.5 pups. In our comparisons, we considered the ratio of the length of the stylopod and zeugopod (S/Z) to normalize for any natural variation in overall embryo size. We measured each limb segment both by the length of ossified bone alone as well as the combined length of the bone and associated cartilage. Across multiple litter comparisons, the average reduction of the S/Z ratio was under 2%. This reduction was not statistically significant using either metric (ossified bone two-way mixed effect ANOVA $F_{1,18}=2.32$, $P=0.145$; combined bone and cartilage ANOVA $F_{1,18}=0.032$, $P=0.859$; Table 1).

DISCUSSION
In this study, we disrupted a major topological interaction partner of the *Pitx1* promoter in the mouse hindlimb. Based on the robustness and tissue specificity of the interaction, we predicted that the PDE would provide substantial quantitative, spatial or temporal regulatory input to *Pitx1*, and that PDE⁻/⁻ mice might exhibit profound molecular and morphological phenotypes due to loss of *Pitx1* expression in the hindlimb. However, our findings show that the deletion of the PDE and the resulting loss of the interaction does not result in reduced viability or recapitulation of the morphological phenotypes of *Pitx1*⁻/⁻ mice (Szeto et al., 1999; Lanctôt et al., 1999). Although we did not observe major spatial or temporal changes in *Pitx1* expression in PDE⁻/⁻ mice, our findings do support that the PDE provides quantitative regulatory input to *Pitx1*. The loss of the PDE results in reduced *Pitx1* expression in both the developing hindlimb and mandibular arch, as well as reduced H3K27ac signal at the *Pitx1* promoter. These findings support that the PDE does enhance *Pitx1* expression in both tissues, although the

more modest reduction of *Pitx1* expression in hindlimb due to PDE loss and our transgenic reporter assay results indicate that the PDE is more active in the mandibular arch than in the hindlimb. However, loss of the PDE is not sufficient to substantially alter hindlimb or jaw morphology in our model, indicating that the development of these structures is robust to moderate reduction in *Pitx1* dosage. It is possible that PDE⁻/⁻ mice exhibit hindlimb or jaw defects at very low penetrance, or subtle phenotypes that might be revealed by detailed morphometric analyses that are beyond the scope of our study (Attanasio et al., 2013).

Compensatory regulatory interactions that buffer *Pitx1* expression against the loss of the PDE might account for the moderate molecular effects of disrupting the PDE-*Pitx1* interaction. These compensatory interactions might involve recruitment of novel enhancers in the *Pitx1* locus or upregulation of enhancers already in use, such as the other interacting enhancers detected by Capture-C (Andrey et al., 2017). We detected no evidence of robust novel interactions or enhancer upregulation in hindlimbs of PDE⁻/⁻ mice. It is possible that transient or weak compensatory interactions might be occurring that our 4C methods are not sensitive enough to detect. However, the absence of a novel robust interaction similar to the PDE-*Pitx1* interaction in PDE⁻/⁻ mice, coupled with the lack of quantitative changes in H3K27ac marking in the *Pitx1* TAD, suggest that *Pitx1* regulatory architecture is largely unchanged by disruption of the PDE. Moreover, any compensatory mechanisms that might exist are necessarily incomplete, as deletion of the PDE has a clear negative effect on *Pitx1* expression levels.

The PDE might thus provide only a moderate contribution to *Pitx1* regulation, despite its prominent interaction with the *Pitx1*
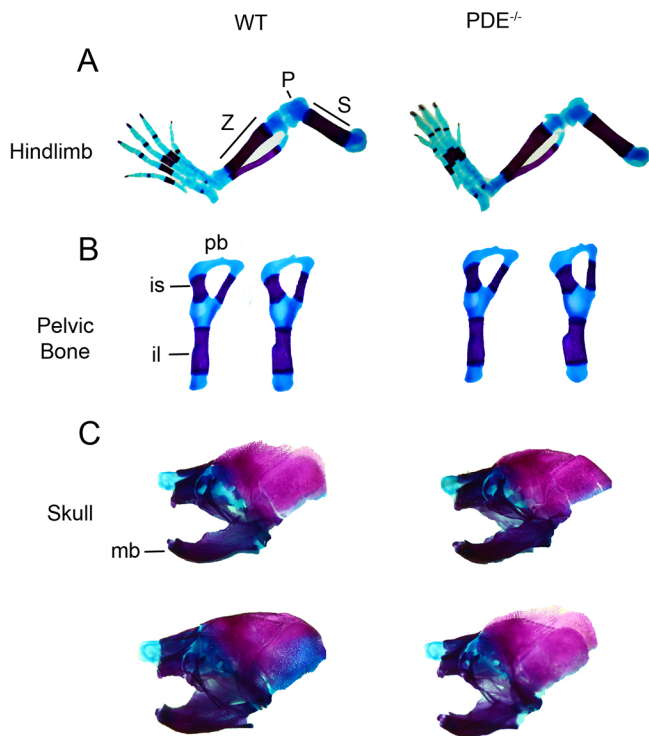
Fig. 5. Comparison of skeletal morphology in wild-type and PDE$^{-/-}$ E18.5 embryos. Representative Alcian Blue (cartilage) and Alizarin Red (bone) skeletal preparations are shown for each genotype. (A) Wild-type and PDE$^{-/-}$ hindlimbs. S, stylopod; Z, zeugopod; P, patella. (B) Pelvic bones from wild-type and PDE$^{-/-}$ mice. il, ilium; is, ischium; pb, pubic bone. (C) Wild-type and PDE$^{-/-}$ skulls. The location of the mandible (mb) is indicated.

promoter. Other regulatory elements in the *Pitx1* locus, which might be partially redundant with the PDE, must determine the spatial, temporal and quantitative expression of *Pitx1*. Regulatory redundancy is an established feature of many developmental genes (Hong et al., 2008; Degenhardt et al., 2010; Frankel et al., 2010; Perry et al., 2010; Montavon et al., 2011; Shlyueva et al., 2014; Cannavò et al., 2016). One recent study supports that combinatorial disruption of multiple redundant enhancers is required to yield molecular or developmental phenotypes for such genes, although this study did not leverage interaction data to select candidate enhancers for deletion as we do here (Osterwalder et al., 2018). Our 4C analysis did not reveal other robust, long-range interactions that might be redundant with the *Pitx1*-PDE interaction

in the hindlimb. However, the interacting enhancers previously detected by Capture-C might nevertheless contribute to *Pitx1* regulation. These enhancers are marked by H3K27ac in both forelimb and hindlimb, but additional hindlimb-specific mechanisms might restrict their impact on *Pitx1* expression to that tissue. Notably, a 44 kb deletion associated with feathered feet in pigeons and reduced *Pitx1* expression in the hindlimb spans the pigeon ortholog of one of these enhancers (Fig. S1) (Domyan et al., 2016). H3K27ac profiles in the hindlimb also suggest that additional enhancers might be located near the *Pitx1* promoter itself. We detected high levels of H3K27ac marking across the *Pitx1* gene body, including intronic marking that might point to proximal enhancers (Fig. 1). Interactions with such proximal elements cannot be distinguished from background in 4C, given their location near the *Pitx1* promoter viewpoint. Other distal enhancers within the *Pitx1* TAD might also act redundantly with the PDE (Fig. 4) by interacting with the *Pitx1* promoter at levels below the sensitivity of chromosome conformation capture methods. These enhancers might be active at earlier time points than those interrogated here or in other studies, and disrupting those elements might have greater effects on *Pitx1* expression.

In light of our results, we speculate that the PDE may nevertheless be crucial for *Pitx1* expression and normal development in ways that cannot be measured in a laboratory setting. The PDE is highly conserved, suggesting it serves an essential function. Redundant enhancers are thought to be maintained by selection in part because they confer a degree of regulatory robustness that buffers developmental gene expression against perturbation (Hong et al., 2008; Perry et al., 2010; Cannavò et al., 2016; Osterwalder et al., 2018). Embryonic development in wild populations is subject to environmental pressures and insults not present in experimental systems. The primary regulatory contribution of the PDE could be to stabilize *Pitx1* expression against variation during development. In the absence of the PDE, *Pitx1* expression might exhibit higher levels of sensitivity to environmental factors or genetic variation, and potentially show much greater changes than we can detect in our model. One approach to address this question in a future study would be to cross PDE null mice with *Pitx1* heterozygous knockout mice, and determine if the resulting compound heterozygotes exhibit more severe phenotypes due to the greater reduction in *Pitx1* dosage (Osterwalder et al., 2018).

Our results have implications for using topology maps to identify crucial regulatory interactions for developmental genes. A primary motivation for generating large-scale maps of topological interactions in the human genome is to discover noncoding variants that contribute to disease by disrupting long-range regulation and perturbing gene expression (Sanyal et al., 2012). However, as the PDE illustrates, robust, tissue-specific interactions may not serve to predict enhancer mutations that have strong effects in model systems. Although it has become commonplace to globally map putative regulatory interactions in multiple biological contexts, we still lack the means to distinguish essential versus redundant interactions *a priori*. This will require large-scale genetic disruption of many interactions, individually and in combination, in order to empirically measure the distribution of effects and characterize the functional diversity of regulatory interactions in the genome.

MATERIALS AND METHODS
Generating PDE conditional knockout alleles using genome editing
All animal work was performed in accordance with approved Yale IACUC protocols. Genetically modified mice were generated at the Yale Genome

Table 1. Comparisons of stylopod/zeugopod (S/Z) length ratios in litter-matched E18.5 wild-type and PDE$^{-/-}$ hindlimbs

	Bone (%)	Bone and cartilage (%)
Litter 1	96.47	92.00
Litter 2	97.45	95.72
Litter 3	94.91	96.27
Litter 4	102.25	105.97
Litter 5	97.29	101.81
Litter 6	101.13	99.25
Average	98.25	98.51
ANOVA	$F_{1,18}$=2.32, P=0.145	$F_{1,18}$=0.032, P=0.859

For each litter, the average S/Z ratio in PDE$^{-/-}$ hindlimbs was divided by the S/Z ratio in wild-type hindlimbs and is expressed as a percentage, with the statistical analysis shown at the bottom.

Editing Center (Yang et al., 2013). sgRNAs were selected for minimal off-target effects based on a CRISPR Design Tool score of >70 (http://crispr.mit.edu/) and the absence of target sites with three or fewer mismatches on the same chromosome (chr13) as the targeted sequence. C57BL/6J zygotes were injected with embryo microinjection buffer (10 mM Tris-HCl pH 7.4, 0.25 mM EDTA) containing two sgRNAs each at 50 ng/μl, Cas9 RNA at 100 ng/μl and two corresponding single-stranded DNA donor sequences both at 100 ng/μl filtered at 0.22 μm before injection (all sequences listed in Table S8). The Cas9 and sgRNA *in vitro* transcription templates were produced via PCR using a px330 plasmid into which the sgRNAs had been cloned as described (Cong et al., 2013) as a template, placing the sequences under control of the T7 promoter. The resulting DNA products were subjected to *in vitro* transcription using the MEGAshortscript T7 Kit (Thermo Fisher Scientific #AM1354) for the sgRNAs and mMESSAGE mMACHINE T7 ULTRA Transcription Kit (Thermo Fisher Scientific #AM1345) for Cas9. The transcribed RNAs were then purified with the MEGAclear Transcription Clean-Up Kit (Thermo Fisher Scientific #AM1908). Primers are described in Table S8.

Resulting F0 mice were backcrossed to wild-type C57BL/6J. To delete the PDE sequence, these mice were then crossed with an actin-Cre C57BL/6J mouse line provided by the Yale Genome Editing Center. All mice used in our analysis were from the F3 generation or later. The PDE knockout line has been deposited as cryopreserved sperm at the Mutant Mouse Resource and Research Center (MMRRC) (ID 43534).

4C analyses in hindlimbs from wild-type and PDE$^{-/-}$ mice

Hindlimbs and forelimbs (100 of each) were dissected from E11.5 C57BL/6J embryos. The tissue was crosslinked and processed in accordance with a protocol adapted from Naumova et al. (2012) and van de Werken et al. (2012) (associated 4C primers are listed in Table S8 and the 4C protocol is provided in the supplementary Materials and Methods). The resulting libraries were prepped and sequenced (1×75 bp) on an Illumina HiSeq 2500. For sequencing, the samples were indexed and multiplexed over two lanes. 30% PhiX control DNA (Illumina) was introduced into each sequencing run to mitigate Illumina sequencing artifacts arising due to the low complexity of PCR-amplified 4C libraries.

After sequencing, the 5′ and 3′ primer sequences were removed from the raw reads using cutadapt (Martin, 2011) (v1.4.1) (cutadapt –discard-untrimmed -g $firstprimer -n 10 -m 10 -O 10) and the trimmed reads were then aligned to the mm9 reference genome using Burrows-Wheeler Aligner (bwa) (Li and Durbin, 2009) (v0.7.10) (bwa mem -t 4). These aligned reads (ranging from 7.5-11 million per replicate) were then used to build a statistical model as described (Klein et al., 2015) modified to incorporate aligned sequence from both ends of paired-end reads. Raw reads were converted to wiggle tracks using BEDTools (Quinlan and Hall, 2010) (v2.17.0) for visualization.

PDE transgenic enhancer assay

We amplified an 8388 bp region [chr13:56056917-56065304 (mm9)] within the PDE with a nested PCR strategy using the primers shown in Table S8. The product was cloned into an *Hsp68-lacZ* reporter vector using Gibson Assembly (NEB #E2611). Generation of transgenic mice and embryo staining were carried out as previously described (Pennacchio et al., 2006).

RT-qPCR analysis of *Pitx1* expression

Hindlimb RNA was collected from five 1:1 litter-matched pairs of mice at four developmental time points: E10.5, E11.5, E12.5 and E13.5 (five litters from each time point, one wild type and one PDE$^{-/-}$ from each litter, 40 total mice considered). RNA was purified from hindlimb pairs from each individual using the miRNeasy Micro Kit (Qiagen #74004) for E10.5 samples and miRNeasy Mini Kit (Qiagen #74106) for all others. RNA quality was measured using an Agilent RNA 6000 Pico chip; all samples analyzed had RIN values ≥8. We used 100 ng total RNA to prepare cDNA from each sample using the Invitrogen Superscript III Reverse Transcription Kit (#18080-051). The resulting cDNA was used in qPCR using Power SYBR Green Mastermix (Thermo Fisher Scientific #4367659) (qPCR

primers listed in Table S8). All samples were run in sets of triplicates reporting the Ct values of *Pitx1* and *Hprt1*, which was used as an internal reference. Reductions in gene expression were calculated by comparing $^{\Delta\Delta}$Ct values of PDE and wild-type samples.

Global transcriptome analyses in hindlimbs and mandibular arch from wild-type and PDE$^{-/-}$ mice

RNA was collected from hindlimb bud pairs of four litter-matched E11.5 mice (two wild type, two PDE$^{-/-}$) generated from a PDE$^{+/-}$×PDE$^{+/-}$ cross. The mandibular arch analysis RNA was derived from three 1:1 pairs of litter-matched E11.5 mice (three litters, one wild type and one PDE$^{-/-}$ from each). RNA was purified using the Qiagen miRNeasy Kit (#74106). Prior to sequencing, RNA quality was analyzed on an Agilent 2100 RNA Pico Chip; all samples submitted for sequencing had RIN values ≥8. RNA was library prepped and sequenced using standard Illumina protocols (2×75 bp) on an Illumina HiSeq 2500 (mandibular arch) and Illumina HiSeq 4000 (hindlimb). Raw reads were aligned to the mm9 transcriptome (GRCm38.p4) using TopHat2 (Kim et al., 2013) (v2.0.9) and Gencode vM.7. Statistical analysis of expression changes was conducted using DESeq2 (Anders and Huber, 2010) using default settings and a false discovery rate (FDR) of 0.1.

Analysis of *Pitx1* expression by *in situ* hybridization

In situ hybridization was performed at E11.5 as previously described (Nagy et al., 2003), using a *Pitx1* probe provided by Jacques Drouin (Lanctôt et al., 1997).

Global profiling of H3K27ac and H3K27me3 in hindlimbs from wild-type and PDE$^{-/-}$ mice

We performed ChIP-seq for each epigenetic mark using chromatin derived from 180 wild-type and 180 PDE$^{-/-}$ hindlimbs (30 per replicate, three replicates per mark) from more than ten litters. Hindlimb tissue was crosslinked, pooled, and sonicated. The pools of each genotype were then split into three ChIP replicates for each epigenetic mark and processed independently for the remainder of the protocol. ChIP-seq of H3K27ac (2 μg/ChIP, Active Motif #39155) and H3K27me3 (5 μg/ChIP, Active Motif #ab4729) was performed as described (Cotney et al., 2012; Cotney and Noonan, 2015). Samples were sequenced (2×75 bp) on an Illumina HiSeq 2500. To control for batch effects, all H3K27ac samples were multiplexed and sequenced on a single lane. The same method was used for H3K27me3 samples. Raw reads were aligned to the mm9 reference genome using Bowtie 2 (v2.2.3) and peaks were called using MACS (Zhang et al., 2008) (v1.4.2).

For quantitative analysis, H3K27ac or H3K27me3 peaks that were reproducible in all three replicates for each genotype were merged. Peaks were considered reproducible if they overlapped by at least 1 bp (identified with the default settings of the intersectBed command in BEDTools). The relative enrichment of H3K27ac and H3K27me3 in these peaks was quantitatively compared using DESeq2 and an FDR of 0.1.

Analyses of skeletal morphology in E18.5 wild-type and PDE$^{-/-}$ mice

E18.5 skeletons were stained with Alcian Blue and Alizarin Red as described (Nagy et al., 2003). Litter-matched mice from six litters were used to obtain 30 wild-type and 24 PDE$^{-/-}$ independent hindlimbs. Bone and cartilage of the stylopod and zeugopod portions of the hindlimb were imaged under a stereo microscope (Leica S6 D) and the segment length measured independently and blinded to genotype by two individuals using Adobe Photoshop CC (2017.0.0). Both left and right limbs were used for these studies.

ANCOVA and ANOVA analyses

To dissect the main effects of the factors contributing to the observed differences in RT-qPCR and limb growth measurements, we analyzed these datasets in comprehensive modeling frameworks. For the RT-qPCR dataset, we employed a three-way mixed effect ANCOVA with $^{\Delta\Delta}$CT measurements as the response variable, 'genotype' as a two-level fixed effect factor, 'embryonic age' (days) as a covariate, and 'litter' as a random effect factor that is nested within 'embryonic age.' For the limb measurements, we used a two-way mixed effect ANOVA with stylopod-to-zeugopod ratio (both accounting for bone

only and for bone and cartilage together) as the response variable, 'genotype' as a two-level fixed effect factor, and 'litter' as a random effect factor. In this way, we were able to isolate the effects of 'genotype,' our factor of interest, from the potential effects of other contributing factors.

Data availability
All associated raw sequence data have been deposited at the Sequence Read Archive (BioProject ID: PRJNA388175).

Supplementary information
Supplementary information available online at
http://dev.biologists.org/lookup/doi/10.1242/dev.158550.supplemental

References

Ahituv, N., Zhu, Y., Visel, A., Holt, A., Afzal, V., Pennacchio, L. A. and Rubin, E. M. (2007). Deletion of ultraconserved elements yields viable mice. *PLoS Biol.* **5**, e234-e236.

Alvarado, D. M., McCall, K., Aferol, H., Silva, M. J., Garbow, J. R., Spees, W. M., Patel, T., Siegel, M., Dobbs, M. B. and Gurnett, C. A. (2011). Pitx1 haploinsufficiency causes clubfoot in humans and a clubfoot-like phenotype in mice. *Hum. Mol. Genet.* **20**, 3943-3952.

Amano, T., Sagai, T., Tanabe, H., Mizushina, Y., Nakazawa, H. and Shiroishi, T. (2009). Chromosomal dynamics at the Shh locus: limb bud-specific differential regulation of competence and active transcription. *Dev. Cell* **16**, 47-57.

Anders, S. and Huber, W. (2010). Differential expression analysis for sequence count data. *Genome Biol.* **11**, R106.

Andrey, G., Schöpflin, R., Jerković, I., Heinrich, V., Ibrahim, D. M., Paliou, C., Hochradel, M., Timmermann, B., Haas, S., Vingron, M. et al. (2017). Characterization of hundreds of regulatory landscapes in developing limbs reveals two regimes of chromatin folding. *Genome Res.* **27**, 223-233.

Attanasio, C., Nord, A. S., Zhu, Y., Blow, M. J., Li, Z., Liberton, D. K., Morrison, H., Plajzer-Frick, I., Holt, A., Hosseini, R. et al., (2013). Fine tuning of craniofacial morphology by distant-acting enhancers. *Science* **342**, 1241006-1241006.

Cannavò, E., Khoueiry, P., Garfield, D. A., Geeleher, P., Zichner, T., Gustafson, E. H., Ciglar, L., Korbel, J. O. and Furlong, E. E. M. (2016). Shadow enhancers are pervasive features of developmental regulatory networks. *Curr. Biol.* **26**, 38-51.

Chan, Y. F., Marks, M. E., Jones, F. C., Villarreal, G., Shapiro, M. D., Brady, S. D., Southwick, A. M., Absher, D. M., Grimwood, J., Schmutz, J. et al. (2010). Adaptive evolution of pelvic reduction in sticklebacks by recurrent deletion of a Pitx1 enhancer. *Science* **327**, 302-305.

Cong, L., Ran, F. A., Cox, D., Lin, S., Barretto, R., Habib, N., Hsu, P. D., Wu, X., Jiang, W., Marraffini, L. A. et al. (2013). Multiplex genome engineering using CRISPR/Cas systems. *Science* **339**, 819-823.

Cotney, J. L. and Noonan, J. P. (2015). Chromatin immunoprecipitation with fixed animal tissues and preparation for high-throughput sequencing. *Cold Spring Harb. Protoc.* **2015**, 191-199.

Cotney, J., Leng, J., Oh, S., DeMare, L. E., Reilly, S. K., Gerstein, M. B. and Noonan, J. P. (2012). Chromatin state signatures associated with tissue-specific gene expression and enhancer activity in the embryonic limb. *Genome Res.* **22**, 1069-1080.

de Laat, W. and Duboule, D. (2013). Topology of mammalian developmental enhancers and their regulatory landscapes. *Nature* **502**, 499-506.

Degenhardt, K. R., Milewski, R. C., Padmanabhan, A., Miller, M., Singh, M. K., Lang, D., Engleka, K. A., Wu, M., Li, J., Zhou, D. et al. (2010). Distinct enhancers at the Pax3 locus can function redundantly to regulate neural tube and neural crest expressions. *Dev. Biol.* **339**, 519-527.

DeMare, L. E., Leng, J., Cotney, J., Reilly, S. K., Yin, J., Sarro, R. and Noonan, J. P. (2013). The genomic landscape of cohesin-associated chromatin interactions. *Genome Res.* **23**, 1224-1234.

Dickel, D. E., Barozzi, I., Zhu, Y., Fukuda-Yuzawa, Y., Osterwalder, M., Mannion, B. J., May, D., Spurrell, C. H., Plajzer-Frick, I., Pickle, C. S. et al. (2016). Genome-wide compendium and functional assessment of in vivo heart enhancers. *Nat. Commun.* **7**, 12923.

Dickel, D. E., Ypsilanti, A. R., Pla, R., Zhu, Y., Barozzi, I., Mannion, B. J., Khin, Y. S., Fukuda-Yuzawa, Y., Plajzer-Frick, I., Pickle, C. S. et al. (2018). Ultraconserved enhancers are required for normal development. *Cell* **172**, 491-499.e15.

Dixon, J. R., Selvaraj, S., Yue, F., Kim, A., Li, Y., Shen, Y., Hu, M., Liu, J. S. and Ren, B. (2012). Topological domains in mammalian genomes identified by analysis of chromatin interactions. *Nature* **485**, 376-380.

Domyan, E. T., Kronenberg, Z., Infante, C. R., Vickrey, A. I., Stringham, S. A., Bruders, R., Guernsey, M. W., Park, S., Payne, J., Beckstead, R. B. et al. (2016). Molecular shifts in limb identity underlie development of feathered feet in two domestic avian species. *eLife* **5**, e12115.

Frankel, N., Davis, G. K., Vargas, D., Wang, S., Payre, F. and Stern, D. L. (2010). Phenotypic robustness conferred by apparently redundant transcriptional enhancers. *Nature* **466**, 490-493.

Fullwood, M. J., Liu, M. H., Pan, Y. F., Liu, J., Xu, H., Mohammed, Y. B., Orlov, Y. L., Velkov, S., Ho, A., Mei, P. H. et al. (2009). An oestrogen-receptor-alpha-bound human chromatin interactome. *Nature* **462**, 58-64.

Ghavi-Helm, Y., Klein, F. A., Pakozdi, T., Ciglar, L., Noordermeer, D., Huber, W. and Furlong, E. E. M. (2014). Enhancer loops appear stable during development and are associated with paused polymerase. *Nature* **512**, 96-100.

Hong, J.-W., Hendrix, D. A. and Levine, M. S. (2008). Shadow enhancers as a source of evolutionary novelty. *Science* **321**, 1314-1314.

Huang, D. W., Sherman, B. T. and Lempicki, R. A. (2008). Systematic and integrative analysis of large gene lists using DAVID bioinformatics resources. *Nat. Protoc.* **4**, 44-57.

Kim, D., Pertea, G., Trapnell, C., Pimentel, H., Kelley, R. and Salzberg, S. L. (2013). TopHat2: accurate alignment of transcriptomes in the presence of insertions, deletions and gene fusions. *Genome Biol.* **14**, R36.

Klein, F. A., Pakozdi, T., Anders, S., Ghavi-Helm, Y., Furlong, E. E. M. and Huber, W. (2015). FourCSeq: analysis of 4C sequencing data. *Bioinformatics* **31**, 3085-3091.

Lanctôt, C., Lamolet, B. and Drouin, J. (1997). The bicoid-related homeoprotein Ptx1 defines the most anterior domain of the embryo and differentiates posterior from anterior lateral mesoderm. *Development* **124**, 2807-2817.

Lanctôt, C., Moreau, A., Chamberland, M., Tremblay, M. L. and Drouin, J. (1999). Hindlimb patterning and mandible development require the Ptx1 gene. *Development* **126**, 1805-1810.

Lettice, L. A., Heaney, S. J. H., Purdie, L. A., Li, L., de Beer, P., Oostra, B. A., Goode, D., Elgar, G., Hill, R. E. and de Graaff, E. (2003). A long-range Shh enhancer regulates expression in the developing limb and fin and is associated with preaxial polydactyly. *Hum. Mol. Genet.* **12**, 1725-1735.

Li, H. and Durbin, R. (2009). Fast and accurate short read alignment with Burrows-Wheeler transform. *Bioinformatics* **25**, 1754-1760.

Logan, M. and Tabin, C. (1999). Role of Pitx1 upstream of Tbx4 in specification of hindlimb identity. *Science* **283**, 1736-1739.

Lupiáñez, D. G., Kraft, K., Heinrich, V., Krawitz, P., Brancati, F., Klopocki, E., Horn, D., Kayserili, H., Opitz, J. M., Laxova, R. et al. (2015). Disruptions of topological chromatin domains cause pathogenic rewiring of gene-enhancer interactions. *Cell* **161**, 1012-1025.

Mann, H. B. and Whitney, D. R. (1947). On a test of whether one of two random variables is stochastically larger than the other. *Ann. Math. Stat.* **18**, 50-60.

Martin, M. (2011). Cutadapt removes adapter sequences from high-throughput sequencing reads. *EMBnet. J.* **17**, 10-12.

Montavon, T., Soshnikova, N., Mascrez, B., Joye, E., Thevenet, L., Splinter, E., de Laat, W., Spitz, F. and Duboule, D. (2011). A regulatory archipelago controls Hox genes transcription in digits. *Cell* **147**, 1132-1145.

Monti, R., Barozzi, I., Osterwalder, M., Lee, E., Kato, M., Garvin, T. H., Plajzer-Frick, I., Pickle, C. S., Akiyama, J. A., Afzal, V. et al. (2017). Limb-Enhancer Genie: An accessible resource of accurate enhancer predictions in the developing limb. *PLoS Comput. Biol.* **13**, e1005720.

Nagy, A., Gertsenstein, M., Vintersten, K. and Behringer, R. (2003). *Manipulating the Mouse Embryo: A Laboratory Manual.* Plainview, NY: Cold Spring Harbor Laboraory Press.

DEVELOPMENT

Naumova, N., Smith, E. M., Zhan, Y. and Dekker, J. (2012). Analysis of long-range chromatin interactions using Chromosome Conformation Capture. *Methods* **58**, 192-203.

Noonan, J. P. and McCallion, A. S. (2010). Genomics of long-range regulatory elements. *Annu. Rev. Genomics Hum. Genet.* **11**, 1-23.

Nora, E. P., Lajoie, B. R., Schulz, E. G., Giorgetti, L., Okamoto, I., Servant, N., Piolot, T., van Berkum, N. L., Meisig, J., Sedat, J. et al. (2012). Spatial partitioning of the regulatory landscape of the X-inactivation centre. *Nature* **485**, 381-385.

Osterwalder, M., Barozzi, I., Tissières, V., Fukuda-Yuzawa, Y., Mannion, B. J., Afzal, S. Y., Lee, E. A., Zhu, Y., Plajzer-Frick, I., Pickle, C. S. et al. (2018). Enhancer redundancy provides phenotypic robustness in mammalian development. *Nature* **554**, 1-27.

Pennacchio, L. A., Ahituv, N., Moses, A. M., Prabhakar, S., Nobrega, M. A., Shoukry, M., Minovitsky, S., Dubchak, I., Holt, A., Lewis, K. D. et al. (2006). In vivo enhancer analysis of human conserved non-coding sequences. *Nature* **444**, 499-502.

Perry, M. W., Boettiger, A. N., Bothma, J. P. and Levine, M. (2010). Shadow enhancers foster robustness of Drosophila gastrulation. *Curr. Biol.* **20**, 1562-1567.

Phillips-Cremins, J. E., Sauria, M. E. G., Sanyal, A., Gerasimova, T. I., Lajoie, B. R., Bell, J. S. K., Ong, C.-T., Hookway, T. A., Guo, C., Sun, Y. et al. (2013). Architectural protein subclasses shape 3D organization of genomes during lineage commitment. *Cell* **153**, 1281-1295.

Quinlan, A. R. and Hall, I. M. (2010). BEDTools: a flexible suite of utilities for comparing genomic features. *Bioinformatics* **26**, 841-842.

Rao, S. S. P., Huntley, M. H., Durand, N. C., Stamenova, E. K., Bochkov, I. D., Robinson, J. T., Sanborn, A. L., Machol, I., Omer, A. D., Lander, E. S. et al. (2014). A 3D map of the human genome at kilobase resolution reveals principles of chromatin looping. *Cell* **159**, 1665-1680.

Sagai, T., Hosoya, M., Mizushina, Y., Tamura, M. and Shiroishi, T. (2005). Elimination of a long-range cis-regulatory module causes complete loss of limb-specific Shh expression and truncation of the mouse limb. *Development* **132**, 797-803.

Sanyal, A., Lajoie, B. R., Jain, G. and Dekker, J. (2012). The long-range interaction landscape of gene promoters. *Nature* **489**, 109-113.

Shlyueva, D., Stampfel, G. and Stark, A. (2014). Transcriptional enhancers: from properties to genome-wide predictions. *Nat. Rev. Genet.* **15**, 272-286.

Siepel, A., Bejerano, G., Pedersen, J. S., Hinrichs, A. S., Hou, M., Rosenbloom, K., Clawson, H., Spieth, J., Hillier, L. W., Richards, S. et al. (2005). Evolutionarily conserved elements in vertebrate, insect, worm and yeast genomes. *Genome Res.* **15**, 1034-1050.

Simonis, M., Klous, P., Splinter, E., Moshkin, Y., Willemsen, R., de Wit, E., van Steensel, B. and de Laat, W. (2006). Nuclear organization of active and inactive chromatin domains uncovered by chromosome conformation capture–on-chip (4C). *Nat. Genet.* **38**, 1348-1354.

Szeto, D. P., Rodriguez-Esteban, C., Ryan, A. K., O'Connell, S. M., Liu, F., Kioussi, C., Gleiberman, A. S., Izpisua Belmonte, J. C. and Rosenfeld, M. G. (1999). Role of the Bicoid-related homeodomain factor Pitx1 in specifying hindlimb morphogenesis and pituitary development. *Genes Dev.* **13**, 484-494.

Tolhuis, B., Palstra, R.-J., Splinter, E., Grosveld, F. and de Laat, W. (2002). Looping and interaction between hypersensitive sites in the active β-globin locus. *Mol. Cell* **10**, 1453-1465.

van de Werken, H. J. G., de Vree, P. J. P., Splinter, E., Holwerda, S. J. B., Klous, P., de Wit, E. and de Laat, W. (2012). 4C technology: protocols and data analysis. *Methods Enzymol.* **513**, 89-112.

Visel, A., Blow, M. J., Li, Z., Zhang, T., Akiyama, J. A., Holt, A., Plajzer-Frick, I., Shoukry, M., Wright, C., Chen, F. et al. (2009). ChIP-seq accurately predicts tissue-specific activity of enhancers. *Nature* **457**, 854-858.

Williamson, I., Lettice, L. A., Hill, R. E. and Bickmore, W. A. (2016). Shh and ZRS enhancer colocalisation is specific to the zone of polarising activity. *Development* **143**, 2994-3001.

Yang, H., Wang, H., Shivalila, C. S., Cheng, A. W., Shi, L. and Jaenisch, R. (2013). One-step generation of mice carrying reporter and conditional alleles by CRISPR/Cas-mediated genome engineering. *Cell* **154**, 1370-1379.

Zhang, Y., Liu, T., Meyer, C. A., Eeckhoute, J., Johnson, D. S., Bernstein, B. E., Nussbaum, C., Myers, R. M., Brown, M., Li, W. et al. (2008). Model-based analysis of ChIP-Seq (MACS). *Genome Biol.* **9**, R137.

DEVELOPMENT